ISSN 0006-2979, Biochemistry (Moscow), 2024, Vol. 89, No. 4, pp. 637-652 © Pleiades Publishing, Ltd., 2024.

Modification of the Hi-C Technology for Molecular Genetic Analysis of Formalin-Fixed Paraffin-Embedded Sections of Tumor Tissues

Maria M. Gridina[1,2,a]*, Yana K. Stepanchuk[1,2], Miroslav A. Nurridinov[1,2], Timofey A. Lagunov[1,2], Nikita Yu. Torgunakov[1,2], Artem A. Shadsky[1,2], Anastasia I. Ryabova[3], Nikolay V. Vasiliev[3], Sergey V. Vtorushin[3,5], Tatyana S. Gerashchenko[3], Evgeny V. Denisov[3], Mikhail A. Travin[4], Maxim A. Korolev[4], and Veniamin S. Fishman[1,2]

[1]*Institute of Cytology and Genetics, Siberian Branch of the Russian Academy of Sciences, 630090 Novosibirsk, Russia*

[2]*Novosibirsk State University, 630090 Novosibirsk, Russia*

[3]*Research Institute of Oncology, Tomsk National Research Medical Center, Russian Academy of Sciences, 634009 Tomsk, Russia*

[4]*Research Institute of Clinical and Experimental Lymphology, Institute of Cytology and Genetics, Siberian Branch of the Russian Academy of Sciences, 630117 Novosibirsk, Russia*

[5]*Siberian State Medical University, Ministry of Health of Russia, 634050 Tomsk, Russia*

[a]*e-mail: gridinam@gmail.com*

Received September 5, 2023
Revised October 31, 2023
Accepted October 31, 2023

Abstract—Molecular genetic analysis of tumor tissues is the most important step towards understanding the mechanisms of cancer development; it is also necessary for the choice of targeted therapy. The Hi-C (high-throughput chromatin conformation capture) technology can be used to detect various types of genomic variants, including balanced chromosomal rearrangements, such as inversions and translocations. We propose a modification of the Hi-C method for the analysis of chromatin contacts in formalin-fixed paraffin-embedded (FFPE) sections of tumor tissues. The developed protocol allows to generate high-quality Hi-C data and detect all types of chromosomal rearrangements. We have analyzed various databases to compile a comprehensive list of translocations that hold clinical importance for the targeted therapy selection. The practical value of molecular genetic testing is its ability to influence the treatment strategies and to provide prognostic insights. Detecting specific chromosomal rearrangements can guide the choice of the targeted therapies, which is a critical aspect of personalized medicine in oncology.

DOI: 10.1134/S0006297924040047

Keywords: chromosomal rearrangements, three-dimensional nuclear organization, oncology, FFPE sections

INTRODUCTION

Together with single nucleotide variants (SNVs), chromosomal rearrangements, including balanced translocations and inversions, play a key role in the pathogenesis of various cancers. Current genomic diagnostic approaches enable genome-wide detection of SNVs and copy number variations, offering significant insights into oncogenic processes. However, efficient detection of balanced chromosomal rearrangements remains elusive. At the same time, these chromosomal rearrangements have been found in almost all types of cancer. Moreover, for some tumors, detection of balanced chromosomal rearrangements is critical for the diagnosis, clarification of prognosis, and choice of therapy.

* To whom correspondence should be addressed.

In many tumors, chromosomal rearrangements not only accompany the process of tumor development, but act as the main cause (driver) of cell oncological transformation. One of the examples is reciprocal translocations observed in Burkitt's lymphoma, in which the translocation of the *MYC* gene from chromosome 8 to chromosome 14 under the influence of the immunoglobulin heavy chain enhancer results in dysregulation of its expression [1]. If breakpoints occur within the genes, this can lead to the gene fusions resulting in the formation of chimeric proteins. Such fusion proteins often involve transcription factors (ERG, MYB) or protein kinases (ABL1, ALK, BRAF, EGFR, JAK2, RET) that play a pivotal role in the oncogenic process. The *TMPRSS2-ERG* gene fusion, which is prevalent in a majority of prostate adenocarcinomas and approximately 20% of high-grade prostate intraepithelial neoplasias, illustrates this mechanism. TMPRSS2 is a serine protease regulated by the androgen-dependent promoter and its fusion with the ERG oncogene results in the ERG overexpression, a key event in the prostate cancer pathogenesis [2]. Similar mechanisms involving *ERG* fusion with other partners, such as *NDRG1*, *EWS*, and *FUS*, have been implicated in other cancer types [3-5].

Gene fusion, a hallmark of various cancers, can dysregulate gene expression and alter the function of the encoded protein. Thus, if gene fusion results in the truncation of one of the fusion partners, this can lead to its overexpression due to the loss of negative regulatory elements (e.g., binding sites for microRNA) or domains determining the protein lifespan. A notable example is the *MYB-NFIB* gene fusion in adenoid cystic carcinoma, resulting from the t(6;9) translocation [6]. In this fusion, the chimeric transcript partially or completely loses a region encoding the C-terminal regulatory domain of MYB containing the sites for protein post-translational modification, as well as a non-coding sequence essential for the binding of microRNAs. Consequently, the absence of these regulatory elements in the MYB portion of the fusion protein leads to the upregulation of *MYB* expression and prolonged protein lifespan [7].

Gene fusions can also lead to the production of chimeric proteins with significantly altered functional domains. In the norm, the FGFR3 receptor tyrosine kinase is activated through the homo/heterodimerization in the presence of fibroblast growth factor (FGF) as a ligand [8]. The translocation between chromosomes 4 and 7 results in the *FGFR3* fusion with *BAIAP2L1*. The resulting chimeric protein possesses the ability for constitutive, ligand-independent homodimerization. This aberrant dimerization is facilitated by the BAR domains of BAIAP2L1, resulting in the FGFR3 kinase activation and potent oncogenic activity [9].

For the diagnostic purposes and long-term storage, tumor samples are preserved as formalin-fixed paraffin-embedded (FFPE) tissue blocks through formalin fixation and subsequent embedding in paraffin. FFPE blocks have many advantages, including stability at room temperature, extended shelf life, and compatibility with immunohistochemical analysis. However, such fixation and storage of samples can lead to the degradation of nucleic acids and appearance of artifacts, which requires optimization of molecular analysis methods [10]. Furthermore, the degradation and modification of nucleic acids in FFPE samples complicate the use of RNA sequencing for the detection of biomarkers [11].

Routine methods for identification of chromosomal rearrangements in tumor tissues include FISH (fluorescence *in situ* hybridization), immunohistochemical analysis, and RT-PCR. These approaches have obvious limitations in the detection of novel or complex chromosome rearrangements. Recent advances in high-throughput sequencing have revolutionized clinical genetics. Whole-genome sequencing (WGS) and whole-exome sequencing (WES) using the short-read technology have excelled in identifying SNVs and unbalanced chromosomal rearrangements, but their accuracy in repetitive genome regions is limited. Detection of balanced rearrangements using WGS and WES depends on the presence of chimeric reads encompassing the rearrangement breakpoints and therefore requires a high sequencing depth. Long-read sequencing methods (PacBio and Oxford Nanopore) are effective for detecting balanced chromosomal rearrangements, but their efficiency diminishes when analyzing FFPE samples due to the DNA degradation. Balanced chromosomal rearrangements often trigger carcinogenesis through two mechanisms: gene fusion and disruption of gene expression resulting from alterations in the gene regulatory environment. Consequently, RNA sequencing has emerged as an important tool for analyzing tumor samples [12-14]. However, this technique demands a high RNA quality, which is challenging when RNA is isolated from FFPE samples [11-16]. Degraded RNA fragments may lack crucial information on the fusion sites. Moreover, RNA-seq technology faces sensitivity issues in the case of low expression of fusion transcripts [13] and fusions with non-coding regions [17] and requires significant sequencing depth (20-30 million paired-end reads) or targeted gene enrichment [11]. The Hi-C (high-throughput chromatin conformation capture) method has been increasingly used in recent years as an alternative approach for detecting various types of chromosomal rearrangements. The advantage of the method is its ability to detect balanced rearrangements at a lower sequencing depth. This efficiency is partly due to the fact that Hi-C does not rely solely on the reads containing the breakpoint. Instead, it analyzes changes in the chromatin contact frequency within broad genomic regions and, therefore,

requires less sequencing depth for the detection of rearrangements [18-27].

Here, we propose a new Hi-C protocol for analyzing material from FFPE tumor sections. We introduced significant modifications to the existing protocols [28, 29], resulting in a highly reproducible technique capable of generating high-quality Hi-C data and detecting all types of chromosomal rearrangements. A key innovation in our approach that distinguishes it from traditional 3C methods, is the use of a sequence-agnostic nuclease, which not only facilitates detection of chromosomal rearrangements but also expands the application of this method to identification of SNVs in clinically significant loci. We have analyzed various databases to compile a comprehensive list of translocations that hold clinical importance for selection of a targeted therapy. The results of modeling conducted in our study demonstrate that our method has a substantial promise for clinical application.

MATERIALS AND METHODS

Analyzed samples. FFPE sections were obtained from patients treated at several medical centers of the Russian Federation. Eight patients were from the Oncology Research Institute of the Tomsk National Medical Research Center. Three patients (age, 43.6 ± 8.62 years) had morphologically verified grade 4 (G4) brain tumors (glioblastoma, giant cell glioblastoma, and diffuse astrocytoma). Five patients (age range, 28-65 years; average age, 50.4 ± 12.9 years) had morphologically confirmed chondrosarcomas of different localization (humerus, femur, tibia, pelvic bones, and sternum); the tumor grades ranged from G2 to G3. Six patients were treated at the Kemerovo Regional Clinical Hospital; three of them had chronic lymphocytic leukemia (CLL) and three patients had large cell lymphoma (LCL). The diagnoses were established based on pathomorphological studies of excisional lymph node biopsies and immunohistochemical verification using a specialized antibody panel.

Tumor tissue samples were collected during surgical procedures. The samples were fixed in 10% neutral buffered formalin for 24 h and embedded in paraffin using standard techniques. For each tumor specimen, 10 μm thick sections were prepared.

FFPE Hi-C. The developed protocol was based on our previously proposed S1 Hi-C method [30] and included the following steps:

1. Deparaffinization:

1.1. An FFPE section was placed in a 1.5-ml tube and 1 ml of lysis buffer Y (150 mM Tris pH 8.0; 140 mM NaCl, 0.5% Igepal, 1% Triton X-100) was added.

1.2. The FFPE section was incubated at 80°C for 3 min.

1.3. Centrifugation was performed at 2500*g* for 5 min.

1.4. The paraffin layer was removed from the solution surface.

1.5. Steps 1.2.-1.4. were repeated (i.e., the total number of incubations was two).

2. Lysis:

2.1. After the second centrifugation, the supernatant was removed and the pellet was resuspended in 1 ml of lysis buffer H (10 mM Tris pH 8.0, 10 mM NaCl, 1% Triton X-100, 0.1% SDC, 20% EtOH).

2.2. The sample was incubated at 45°C overnight.

2.3. Centrifugation was performed at 2500*g* for 5 min.

2.4. The precipitate was washed once with 1 ml of lysis buffer Y.

2.5. The sample was incubated in 1 ml of lysis buffer Y for 1 h at room temperature on an orbital shaker.

2.6. Centrifugation was performed at 2500*g* for 5 min.

2.7. The supernatant was removed, and the pellet was resuspended in 500 μl of lysis buffer D (50 mM Tris pH 7.5, 0.5 mM $CaCl_2$, 0.3% SDS).

2.8. The sample was incubated at 37°C for 1 h.

2.9. SDS was quenched by adding 91 μl of 10% Triton X-100 for 10 min at room temperature.

2.10. Centrifugation was performed at 2500*g* for 5 min.

2.11. The pellet was washed once with 500 μl of 1× S1 nuclease buffer (Thermo Scientific) containing 1% Triton X-100.

3. Chromatin fragmentation:

3.1. The pellet was resuspended in 80 μl of 1× S1 nuclease buffer.

3.2. 200 U of S1 nuclease (Thermo Scientific) was added and the mixture was incubated at 37°C for 1 h.

3.3. The reaction was stopped by adding 5 μl of 500 mM EDTA and purified with 1 volume of AMPure magnetic beads according to the manufacturer's recommendations.

3.4. Chromatin associated with magnetic beads was resuspended in 100 μl of H_2O (chromatin remained bound to the beads until the DNA isolation stage).

4. Further steps, including biotin labeling, ligation, DNA isolation, ligation fragment enrichment, and preparation of NGS libraries, were performed according to the protocol described by Gridina et al. [31]. DNA quantity was determined with a Qubit dsDNA HS Assay Kit.

The prepared libraries were sequenced using the BGI sequencing platform with 150-bp paired-end reads. The sequencing depth was 10-100 thousand reads per sample for shallow sequencing and ~80 million paired-end reads for deep sequencing.

Modeling of chromosomal rearrangements was performed with the Charm software (https://github.com/genomech/Charm/) using the published results of genome-wide Hi-C studies in IMR90 cells [32] (identifiers SRR1658675, SRR1658676, SRR1658679) to create a database of reference contacts. Each chromosomal rearrangement was modeled as heterozygous, with a total number of ~30 million Hi-C contacts. The coordinates for the boundaries of modeled chromosomal rearrangements (Online Resource 1) were rounded to the nearest 5 kb. Rearrangements smaller than 25 kb were scaled up to this threshold.

Construction of contact maps and analysis of quality metrics of Hi-C libraries. Analysis of Hi-C data and construction of Hi-C heatmaps were conducted as outlined in [31]. A modified version of the Juicer software version 1.6 (available on GitHub: https://github.com/genomech/juicer1.6_compact) was used to calculate the quality scores.

RESULTS

D**evelopment of Hi-C protocol for FFPE samples using S1 nuclease.** The majority of published Hi-C protocols have been designed for living cells or fresh tissues [19, 31-33]; few of them were adapted for frozen samples [34]. While these protocols have been well-established for the respective sample types, with known details and critical points [35-37], their applicability to FFPE tumor sections is limited. Currently, there are only two Hi-C protocols for the analysis of FFPE sections [28, 29]. We compared these two existing protocols (Table 1) and identified significant methodological differences, particularly, at the deparaffinization and sample lysis stages. For deparaffinization, Troll et al. [28] recommended xylene treatment followed by alcohol washing, while Allahyar et al. [29] suggested a 3-min incubation at 80°C, centrifugation, and removal of the paraffin layer. After deparaffinization, in order to ensure the availability of chromatin for restriction enzymes, Troll et al. treated the samples with proteinase K (0.5 mg/ml for 1 h at 37°C), whereas Allahyar et al. used sonication and subsequent incubation for 2 h at 80°C. Both proteinase treatment and prolonged incubation at 80°C can lead to the destruction of cross-links formed by formaldehyde [38] and DNA release from the chromatin. Finally, both studies suggested using restriction endonucleases with four-nucleotide recognition sites for chromatin fragmentation. However, this approach can result in a low coverage of genomic regions distant from the enzyme recognition sites, which might limit identification of certain genomic variants, such as SNVs in the oncogene exons located far from the restriction sites.

We have developed a modified Hi-C protocol specifically designed for preparing libraries from FFPE sections (Table 1). The lysis conditions were adjusted to be less harsh, and we used S1 nuclease instead of restriction endonucleases (see Materials and methods) to provide uniform genome coverage [30].

During the preparation of the Hi-C libraries from living cells or tissues, the quality of DNA fragments is tested after the following key steps:

1. Post-lysis, pre-fragmentation;
2. Post-fragmentation, pre-ligation;
3. Post-ligation.

These control checkpoints are crucial for evaluating the quality of prepared libraries (Fig. 1, a, b). Before fragmentation, a band corresponding to the high-molecular-weight DNA should be detected, which disappears after fragmentation with the formation of many low-molecular fragments of various lengths. After ligation, the distribution of fragment lengths shifts to a higher molecular weight region.

We found that the standard quality controls typically employed in the Hi-C library preparation from living tissues were not applicable or representative

Table 1. Comparison of FFPE Hi-C protocols

Steps	Conditions		
	Troll et al. [28]	Allahyar et al. [29]	Our protocol
Deparaffinization	xylene	3 min at 80°C, centrifugation	3 min at 80°C, centrifugation
Lysis	proteinase K, 1 h at 37°C	0.6% SDS, sonication, incubation at 80°C for 2 h	lysis in the presence of ionic and nonionic detergents
Chromatin fragmentation	*Mbo*I, 1 h at 37°C	*Nla*III, 1 h at 37°C	S1 nuclease, 1 h at 37°C
Biotin labeling	+	–	+
Ligation	2 h, room temperature	1 h, 16°C	overnight, 16°C
Ligation product enrichment	+	–	+

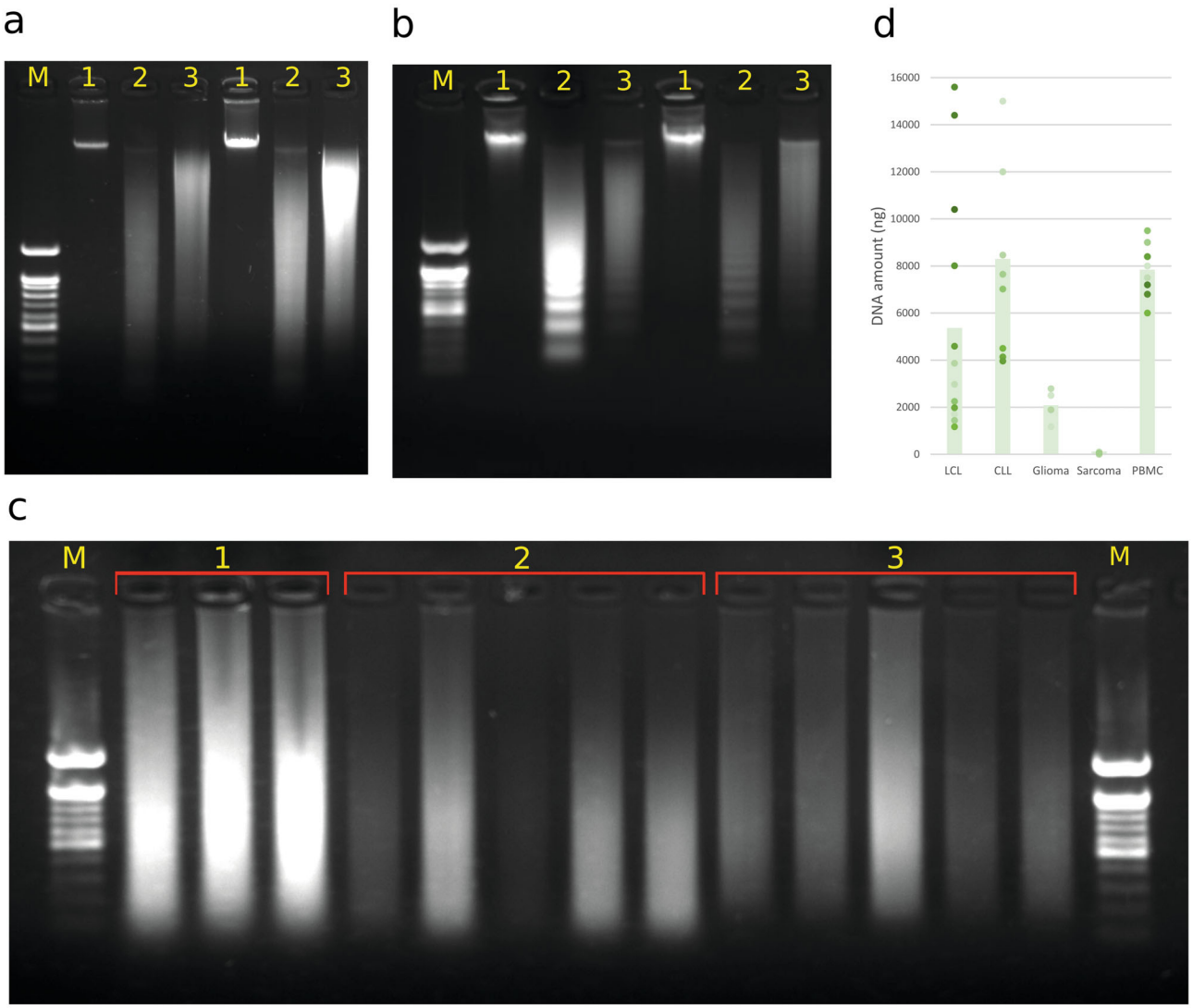

Fig. 1. Results of chromatin digestion and ligation in Hi-C experiments in living cells and tissues using *Dpn*II (a) and S1 nuclease (b) and in FFPE sections using our protocol (c). Lanes: 1, pre-fragmentation, 2, post fragmentation, 3, post-ligation; M, 100-bp ladder (SibEnzyme). d) DNA quantification (ng) in Hi-C libraries obtained from cells and FFPE sections of different tumor types. The number of analyzed libraries from peripheral blood mononuclear cells (PBMCs) was 16, from FFPE sections: LCL – 13, CLL – 9, gliomas – 4, sarcomas – 5.

in the case of FFPE samples. Long-term fixation of tumor tissues in formaldehyde and subsequent embedding in a paraffin block lead to a significant DNA degradation [39, 40]. Consequently, DNA extracted from FFPE blocks is already in a highly fragmented state. According to our data, further nuclease treatment and ligation do not result in contrasting changes in the fragment length (Fig. 1c). However, our analysis of the sequencing data quality and visual examination of the resulting FFPE Hi-C maps indicated successful completion of the key Hi-C protocol stages. For instance, the Hi-C libraries represented in Fig. 1, as well as additional libraries detailed in Online Resource 2 (samples s11-s15), demonstrated acceptable quality metrics. Hence, we believe that in the case of FFPE Hi-C, the described controls are not necessary. Instead, we recommend assessing the library quality based on the results of shallow sequencing.

Unlike the FFPE Hi-C method, Hi-C analysis of live cells using restriction endonuclease *Dpn*II or S1 nuclease allows to easily vary the amount of the starting material, while in the case of FFPE sections, accurate estimation of the number of cells in each section can be a challenge. We observed a significant variability in the amount of DNA isolated from FFPE samples of different tumors, as well as in the samples of the same tumor type (Fig. 1d). Thus, FFPE sections from sarcomas consistently yielded the lowest amount of DNA, which forced us to utilize three FFPE sections from a single block for analysis. Therefore, we recommend to determine the required number of sections for each tumor type to obtain sufficient yield of DNA libraries.

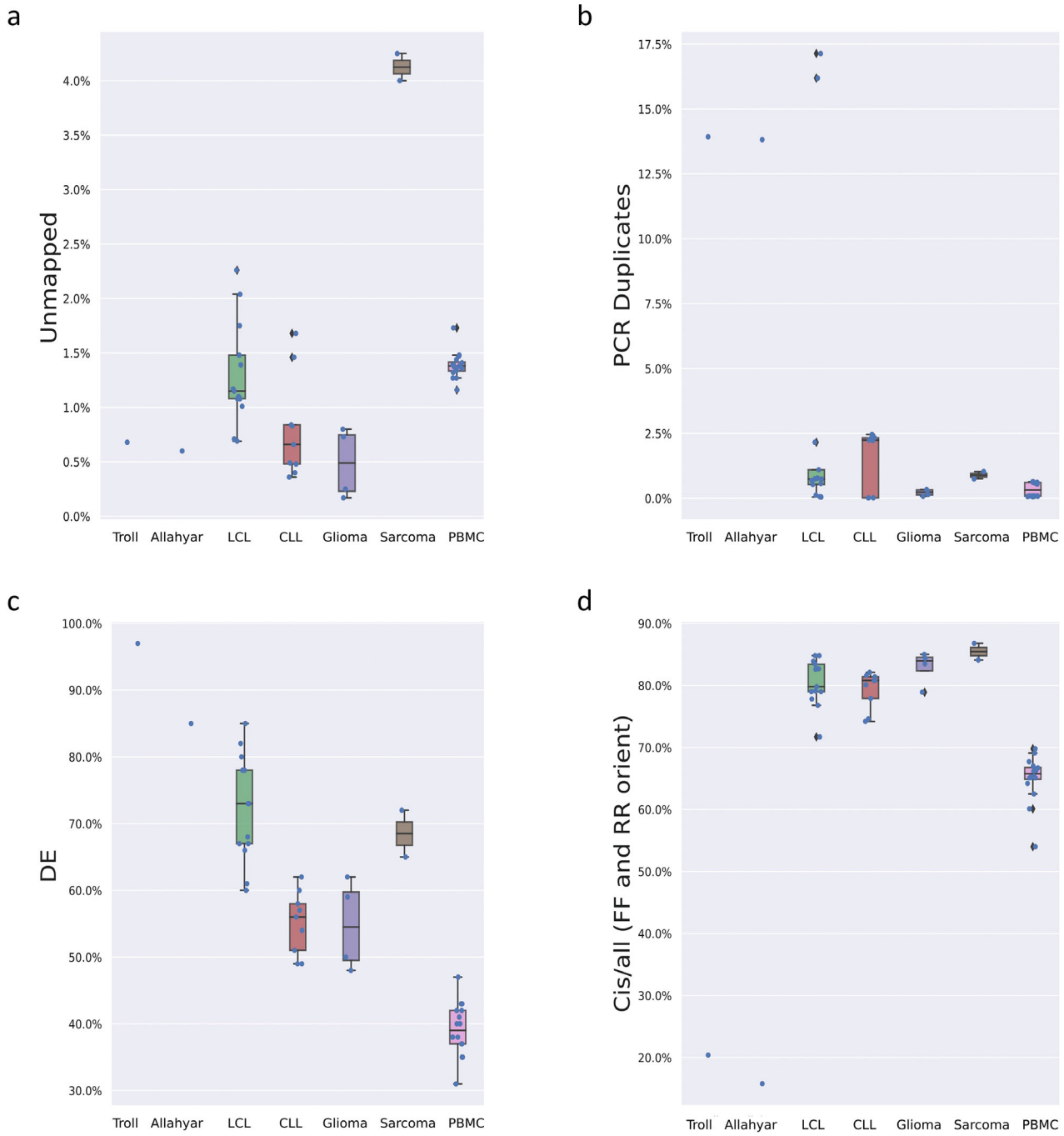

Fig. 2. Quality metrics of FFPE Hi-C datasets showing proportion of unmapped reads (a), proportion of PCR duplicates (b), proportion of DEs (c), proportion of *cis* contacts among all Hi-C contacts (d). Each dot represents an independent Hi-C library preparation. The number of analyzed libraries from PBMCs was 16 and from FFPE sections: LCL – 13, CLL – 9, gliomas – 4, sarcomas – 2.

Using the newly developed protocol, we prepared FFPE Hi-C libraries from CLL, LCL, gliomas, and sarcoma samples. The CLL sections were also used to construct the libraries according to the protocols suggested by Troll et al. [28] and Allahyar et al. [29]. After sequencing, the libraries were assessed for their quality. We observed a low number of unmapped reads and PCR duplicates across all the libraries (Fig. 2, a and b, respectively). Another key quality metric for Hi-C libraries is a proportion of dangling ends (DEs), uninformative fragments that are not ligation products. The DE content in the Hi-C libraries prepared from peripheral blood mononuclear cells (PBMCs) using S1 nuclease averaged 40%. However, in the FFPE Hi-C libraries prepared according to the developed protocol, this proportion was higher and varied depending on the tumor type. The highest DE content was observed in the libraries prepared following the protocols of

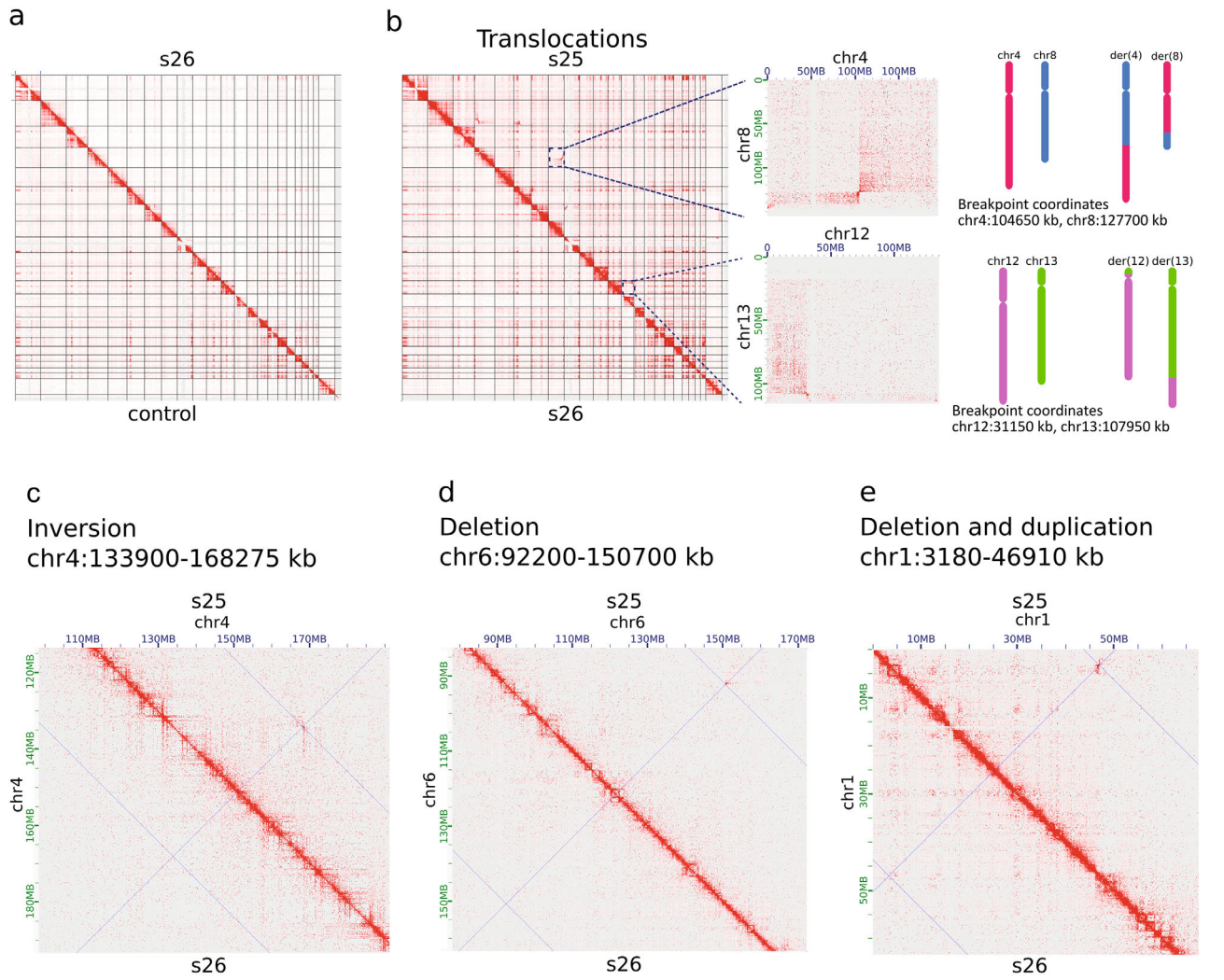

Fig. 3. Representative Hi-C data obtained for FFPE sections using the developed protocol. a) Chromosome-scale Hi-C heatmap for sample s26 (above the diagonal) and the map obtained for blood lymphocytes (control; below the diagonal) [30]. b) Examples of contact patterns in Hi-C maps and their schematic representation: reciprocal translocations (b), inversions (c), heterozygous deletions (d), heterozygous deletions and duplications (e). In panels (b-e), above the diagonal, contact map for sample s25; below the diagonal, contact map for s26 (control).

Troll et al. [28] and Allahyar et al. (Fig. 2c). We have previously shown [31] that the most important metric of the library quality is a proportion of *cis* contacts [*cis*/all ratio (FF and RR orient)], which reflects the proportion of Hi-C reads aligned to the same chromosome. Thus, a low proportion of *cis* contacts may result from the reversal of cross-links and subsequent random ligation of released DNA. For all the libraries prepared using our protocol, the proportion of *cis* contacts was above 70%, while for the libraries prepared according to Troll et al. and Allahyar et al., it was 20 and 15%, respectively (Fig. 2d).

However, it was not the aim of our study to compare between our FFPE Hi-C protocol and protocols proposed by Troll et al. [28] and Allahyar et al. [29], as the latter ones utilize enzymes with specific recognition sites, which limits their capacity to identify genomic variants with the efficacy that can be achieved with our protocol, which uses S1 nuclease [31, 41]. Therefore, we have not used the protocols by Troll et al. [28] and Allahyar et al. [29] for a larger set of samples or different tumor types. Although the obtained data did not allow us to draw a statistical comparison of the quality of Hi-C data obtained by different protocols, we can still state a higher quality of Hi-C libraries obtained using our protocol.

Two libraries were subjected to deep sequencing and the results obtained were used to construct heatmaps of the Hi-C contacts, which revealed distinct patterns indicating various types of chromosomal rearrangements (Fig. 3, a-e). We were able to detect all types of chromosomal structural rearrangements, such as deletions, duplications, inversions, and translocations. Based on these findings, we can conclude that the developed method for FFPE Hi-C analysis using S1 nuclease was effective in generating maps of three-

dimensional chromatin contacts and identifying chromosomal rearrangements based on the obtained data.

Prospects of FFPE Hi-C analysis in the selection of targeted therapy in oncological diseases. The developed FFPE Hi-C protocol has a significant potential for future clinical applications, as it can detect chromosomal rearrangements (translocations and inversions), including balanced ones. These rearrangements are often challenging to identify using standard sequencing methods. The practical value of molecular genetic testing lies in its ability to influence patient treatment strategies and provide prognostic insights. Detection of specific chromosomal rearrangements can guide the choice of targeted therapy, which is a critical aspect of personalized medicine and oncology. To determine the scope of applications for our method, we analyzed the databases of the National Cancer Institute (https://www.cancer.gov/about-cancer/treatment/drugs/cancer-type), CIViC (https://civicdb.org/welcome), and MyCancerGenome (https://www.mycancergenome.org/). We identified balanced chromosomal rearrangements leading to the gene fusions resulting in the generation of chimeric products that have been already targeted in existing or developed therapies (Table 2). Our analysis revealed that the highest number of gene fusions for which the targeted therapy had been developed has been described for hematological oncological diseases and, in the case of solid tumors, for various types of sarcomas and lung cancer. These diseases also exhibit the greatest diversity of fusion partners. Thus, several fusion variants have been identified in melanoma and cholangiocarcinoma; however, in each of the fusions, one of the partners remained the same: BRAF in melanoma and FGFR2 in cholangiocarcinoma.

In addition to the translocations listed in Table 2, there are other rearrangements that are important for establishing a diagnosis and/or prognosis, but do not currently have approved targeted drugs. For instance, KMT2A/MLL gene fusions frequently observed in patients with acute leukemia, are known to be associated with a poor prognosis [42]. The list of clinically relevant gene fusions will expand with the discovery of new gene fusions and approval of novel therapeutic drugs.

In order to assess the possibility of detecting chromosomal rearrangements described in Table 2, we simulated the results of the FFPE Hi-C experiment using the Charm tool (https://github.com/NuriddinovMA/Charm). The simulated Hi-C experiments focused on 5 inversions and 7 translocations from Table 2 (Online Resource 1). The models corresponded to the FFPE Hi-C libraries sequenced with a depth of about 30 million paired-end reads. For each translocation, we generated two models: one showed a reciprocal translocation and the other showed a translocation of the minimal-size fragment sufficient to form a chimeric protein, i.e., a translocation of a region from the 3′-end of the fused gene to the breakpoint (Fig. 4a). The size of the simulated inversions ranged from 2.3 to 79.9 million bp, while the translocations varied in size from 7.9 to 109 kb. The Hi-C contact heatmaps of clearly displayed all simulated chromosomal rearrangements (Fig. 4, b-e; Online Resource 3). This result suggests that the Hi-C analysis of FFPE samples has a high potential in detecting known clinically significant chromosomal rearrangements.

DISCUSSION

In this work, we proposed a protocol for the Hi-C analysis of FFPE tumor sections using S1 nuclease and demonstrated that this method can be applied for detecting various types of chromosomal rearrangements. To fully assess the power of the method, it is crucial to compare it against other high-throughput diagnostic techniques in terms of several key factors, such as time, complexity, cost, and accuracy of analysis. Our protocol can be implemented using standard laboratory equipment commonly used for the preparation of whole-genome libraries. The process of sample preparation took 2 more days compared to WGS; however, the main time-consuming procedure was developing the logistics for sample pooling and sequencing rather than sample preparation itself. According to our estimates, the cost of FFPE Hi-C exceeds the cost of WGS by no more than 20%. A future direction for our research will be understanding the characteristics and limitations of the FFPE Hi-C method. We still have to evaluate the sensitivity and specificity of this method, its ability to determine the proportion of tumor cells in a sample, and the amount of input material required for different types of tumors. Then, it will be possible to fully compare the proposed FFPE Hi-C protocol with the existing high-throughput diagnostic methods.

The high-throughput sequencing technology has opened a new era of personalized therapy for oncology patients. It has dramatically enhanced our ability to understand various oncological diseases at a molecular level. However, it still remains unclear which sequencing methods and when should be used in daily clinical practice. In 2020, the European Society of Medical Oncology recommended routine use of high-throughput sequencing methods for the diagnostics of non-squamous non-small cell lung cancer, prostate adenocarcinoma, ovarian carcinoma, and cholangiocarcinoma [43]. Despite this limited list, the use of high-throughput sequencing methods may be worthwhile for other types of cancer, as it can clarify the diagnosis and even change the treatment regimen.

A compelling example of the practical application of NGS methods for detection of chromosomal

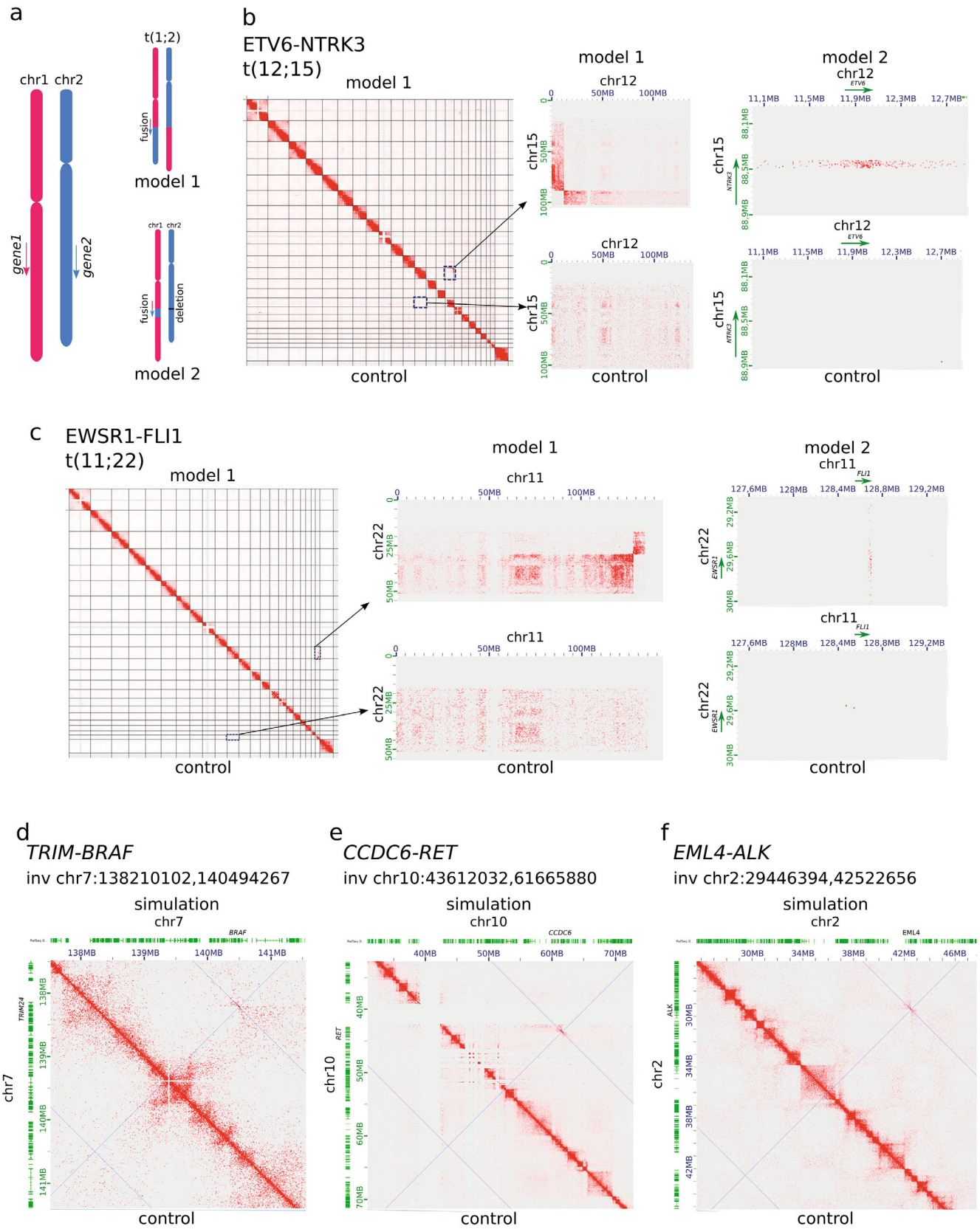

Fig. 4. Simulation of chromosomal rearrangements. a) Schematic representation of two variants of translocation leading to the gene fusion. b and c) Simulated FFPE Hi-C heatmaps for translocations. d-f) Simulated FFPE Hi-C heatmaps for inversions. Above the diagonal, simulated heatmap; below diagonal, control (simulated FFPE Hi-C map with no structural variations and with the same number of contacts as the simulated map with the rearrangement).

Table 2. List of balanced chromosomal rearrangements and gene fusions with developed targeted therapy

Rearrangement	Fusion partners		Targeted therapy drugs	Diagnosis
	A	B		
t(9;22)(q34;q11)	*ABL1*	*BCR*	Dasatinib, Imatinib, Nilotinib, Bosutinib, Bafetinib, Asciminib	acute lymphocytic leukemia, acute myeloid leukemia, chronic myelogenous leukemia
t(9;12)(q34;p13)		*ETV6*	Imatinib, Dasatinib, Nilotinib	B-lymphoblastic leukemia/lymphoma
t(3;9)(p13;q34)		*FOXP1*	Dasatinib	B-lymphoblastic leukemia/lymphoma
t(2;9)(q12;q34)		*RANBP2*	Dasatinib	B-lymphoblastic leukemia/lymphoma
t(1;9)(q24;q34)		*RCSD1*	Dasatinib, Imatinib, Ponatinib	B-lymphoblastic leukemia/lymphoma
t(1;9)(p34;q34)		*SFPQ*	Dasatinib, Imatinib	acute lymphocytic leukemia, B-lymphoblastic leukemia/lymphoma
t(5;9)(q23;q34)		*SNX2*	Dasatinib, Imatinib	B-lymphoblastic leukemia/lymphoma
inv(1)(q24q25)	*ABL2*	*RCSD1*	Imatinib	B-lymphoblastic leukemia/lymphoma
t(1;7)(q25;q34)		*ZC3HAV1*	Imatinib	B-lymphoblastic leukemia/lymphoma
	ALK	different	ALK signaling pathway inhibitors, HSP90 inhibitors, EGFR tyrosine kinase inhibitors, Crizotinib, Brigatinib, Alectinib, Ceritinib, Entrectinib, Pemetrexed, 17-AAG*	breast cancer, colorectal adenocarcinoma, epithelioid inflammation, myofibroblastic sarcoma, inflammatory myofibroblastic tumor, lung adenocarcinoma, non-small cell lung cancer, thyroid carcinoma, vaginal sarcoma, anaplastic large cell lymphoma, diffuse large B-cell lymphoma
inv(2)(p23;p23)		*CAD*	Entrectinib	colorectal cancer
t(2;17)(p23;q23)		*CLTC*	Crizotinib	diffuse large B-cell lymphoma
inv(2)(p23p21)		*EML4*	17-AAG*, Alectinib (CH5424802), AUY922*, Ceritinib, Crizotinib, Brigatinib, IPI-504*, Erlotinib, Lorlatinib	acinar adenocarcinoma of the lung, non-small cell lung cancer, renal cell carcinoma
t(2;7)(p23;q11)		*HIP1*	Crizotinib, Alectinib	non-small cell lung cancer
t(2;5)(p23;q35)		*NPM*	Crizotinib	anaplastic large cell lymphoma
inv(2)(p23q13)		*RANBP2*	Crizotinib	inflammatory myofibroblastic tumor
inv(2)(q21;q22)	*ASNS*	*KMT2E*	Asparaginase	T-cell lymphoblastic leukemia
t(X;17)(p11;q25)	*TFE3*	*ASPL*	Cabozantinib, Dasatinib	alveolar soft tissue sarcoma
	BRAF	different	Cobimetinib, Trametinib	melanoma, ovarian cancer
inv(7)(q34;q34)		*AGK*	Sorafenib, Vemurafenib	melanoma
inv(7)(q21q34)		*AKAP9*	MEK inhibitors	papillary thyroid cancer

Table 2 (*cont.*)

Rearrangement	Fusion partners		Targeted therapy drugs	Diagnosis
	A	B		
inv(7)(q34;q36)	*BRAF*	*CUL1*	MEK inhibitors	serous ovarian carcinoma
inv(7)(q22;q34)		*CUX1*	Vemurafenib	pancreas cancer
t(1;7)(p31;q34)		*MIGA1*	BRAF Inhibitor, HL-085	Langerhans cell histiocytosis
inv(7)(q32;q34)		*NRF1*	Trametinib	transitional cell carcinoma
inv(7)(q33;q34)		*TRIM24*	Vemurafenib	melanoma
inv(7)(q22;q34)		*ZKSCAN1*	Trametinib	melanoma
t(7;11)(q34;p15)		*PPFIBP2*	Trametinib	melanoma
t(4;7)(q25;q34)		*PAPSS1*	Trametinib, Vemurafenib	melanoma
t(15;19)(q14;p13)	*BRD4*	*NUTM1*	Birabresib	NUT midline carcinoma
t(X;14)(p22;q32)	*CRLF2*	*IGH*	Ruxolitinib	pediatric B-cell acute lymphoblastic leukemia, adult B-cell acute lymphoblastic leukemia
t(1;5)(q22;q32)	*CSF1R*	*MEF2D*	Imatinib	acute lymphocytic leukemia
t(X;6)(q28;p22)	*DEK*	*AFF2*	Pembrolizumab	head and neck cancer
t(7;15)(p11;q15)	*EGFR*	*RAD51*	Erlotinib, Osimertinib, Icotinib, Afatinib	lung adenocarcinoma
	EWSR1	different	TK216*	soft tissue sarcoma
t(12;22)(q13;12)		*ATF1*	Crizotinib	clear cell sarcoma
t(11;22)(q24;q12)		*FLI1*	genotoxic chemotherapies	Ewing sarcoma
t(9;22)(q22;q12)		*NR4A3*	Pazopanib, Sunitinib	extraskeletal myxoid chondrosarcoma
inv(8)(p11;p11)	*FGFR1*	*BAG4*	AZD4547*	carcinoma
t(8;12)(p11;p11)		*FGFR1OP2*	Ponatinib	acute myeloid leukemia
t(8;13)(p11;q11)		*ZNF198*	Midostaurin	chronic myeloproliferative disease
	FGFR2	different	BGJ-398 (Infigratinib), AZD4575*, JNJ-42756493 (Balversa), Debio1347*, Futibatinib, Erdafitinib, Infigratinib, Phosphate, Pemigatinib	cholangiocarcinoma, bladder cancer
t(1;10)(p13;q26)		*AHCYL1*	BGJ398	cholangiocarcinoma
inv(10)(q21;q26)		*BICC1*	BGJ398, JNJ-42756493	cholangiocarcinoma, endometrial cancer, urothelial carcinoma
t(4;10)(p16;q26)		*TACC3*	Pazopanib, Ponatinib	cholangiocarcinoma

Table 2 (*cont.*)

Rearrangement	Fusion partners		Targeted therapy drugs	Diagnosis
	A	B		
	FGFR3	different	FGFR signaling blockers, TORC1/2 inhibitors, AZD4547*, JNJ-42756493, BGJ398, Debio1347*, Erdafitinib	bladder cancer
	FLT3	different	FLT3 signaling blockers, Sorafenib, all-*trans* retinoic acid, Anthracycline*, Daunorubicin*, Lestaurtinib, Selumetinib (AZD6244)	acute myeloid leukemia
t(2;13)(q36;q14)	*FOXO1*	*PAX3*	Thapsigargin	alveolar rhabdomyosarcoma
t(9;22)(p24;q11)	*JAK2*	*BCR*	Ruxolitinib	myeloid neoplasm
t(9;14)(p24;q32)		*GOLGA5*	Ruxolitinib	b-lymphoblastic leukemia/lymphoma
t(8;9)(p22;p24)		*PCM1*	Ruxolitinib	leukemia
t(5;9)(q14;p24)		*SSBP2*	Ruxolitinib	B-lymphoblastic leukemia/lymphoma
	KIT	different	Imatinib	malignant melanoma of the rectum
inv(7)(q22;q31)	*MET*	*ATXN7L1*	Crizotinib	non-small cell lung cancer
t(7;10)(q31;p11)		*KIF5B*	Crizotinib	Non-small cell lung cancer
t(7;8)(q31;p12)		*RBPMS*	Cabozantinib	congenital fibrosarcoma
t(8;21)(q24,p12)	*NRG1*	*APP*	Afatinib	–
t(1;8)(q24;p12)		*ATP1B1*	Afatinib	cholangiocarcinoma, pancreatic ductal adenocarcinoma
t(5;8)(q33;p12)		*CD74*	Afatinib	mucinous adenocarcinoma
t(8;11)(p12;q12)		*SLC3A2*	Afatinib, Erlotinib, Lumretuzumab	lung adenocarcinoma, mucinous adeno-carcinoma
t(8;20)(p12q13)		*SDC4*	Afatinib	lung adenocarcinoma
	NTRK1	different	ARRY-470, Entrectinib, Larotrectinib (LOXO-101), LESTAURTINIB*, Crizotinib	colorectal cancer, sarcoma, all solid tumors, lung adenocarcinoma
t(1;12)(q23;p13)		*ETV6*	Entrectinib	all types
t(1;5)(q23;q35)		*SQSTM1*	Entrectinib	non-small cell lung cancer
inv(1)(q21q23)		*TPM3*	Larotrectinib, Entrectinib	Sarcoma, papillary thyroid cancer
inv(1)(q23q31)		*TPR*	Larotrectinib	all solid tumors
	NTRK2	different	Larotrectinib, Entrectinib	all solid tumors

Table 2 (*cont.*)

Rearrangement	Fusion partners		Targeted therapy drugs	Diagnosis
	A	B		
	NTRK3	different	Entrectinib, Larotrectinib, blockers of PI3K, SRC, and IGF1 signaling pathways	all solid tumors
t(12;15)(p13;q25)		*ETV6*	Entrectinib, Etoposide, Larotrectinib, Crizotinib	salivary gland carcinoma, breast cancer, congenital mesoblastic nephroma, B-lymphoblastic leukemia/lymphoma
	PDGFRA	different	Imatinib	myelodysplasia, myeloproliferative neoplasms
t(4;22)(q12;q11)		*BCR*	Imatinib	B-cell acute lymphoblastic leukemia
	PDGFRB	different	Imatinib	chronic myeloproliferative disease, dermatofibrosarcoma, myelodysplasia, myeloproliferative neoplasm, acute lymphocytic leukemia
t(12;17)(p13;q21)		*ATF7IP*	Dasatinib, Imatinib, Nilotinib, Ponatinib, Bafetinib, Rebastinib	pediatric B-cell acute lymphoblastic leukemia
t(17;22)(q21;q13)		*COL1A1*	Sunitinib	dermatofibrosarcoma
t(15;17)(q22;q21)	*PML*	*RARA*	Tretinoin, arsenic trioxide, all-*trans*-retinoic acid	acute promyelocytic leukemia
	RET	different	Cabozantinib, Vandetanib, Pralsetinib, Selpercatinib	non-small cell lung cancer, thyroid cancer
inv(10)(q11q21)		*CCDC6*	Nintedanib, Agerafenib, Pralsetinib	non-small cell lung cancer, colorectal cancer, solid tumors
inv(10)(p11q11)		*KIF5B*	Vandetanib, Selpercatinib, Everolimus, Pralsetinib	lung adenocarcinoma, solid tumors
	ROS1	different	Ceritinib, Entrectinib, Erlotinib, Gefitinib	lung adenocarcinoma, bronchioloalveolar adenocarcinoma, colorectal adenocarcinoma, non-small cell lung cancer
t(5;6)(q33;q22)		*CD74*	Cabozantinib, Crizotinib, Brigatinib, Ceritinib, Foretinib, Lorlatinib,	non-small cell lung carcinoma, lung adenocarcinoma
t(3;6)(q12;q22)		*TFG*	Crizotinib	inflammatory myofibroblastic tumor
	RSPO2	different	Wnt signaling inhibitors, CGX1321	digestive system cancer

Note. We call the fusion partner "A" the gene, the changes in the activity of which lead to the disease development.

* At the clinical trial stage.

rearrangements in clinical oncology was reported by Hehir-Kwa et al. [44]. Based on histological analysis of brain tumor, a one-year-old child was diagnosed with glioblastoma. In accordance with the diagnosis, the treatment was started using the HGG HIT protocol for infants. After 6 weeks of active tumor growth, the protocol was changed to BBSFOP HGG. DNA methylation analysis allowed the tumor to be classified as a glioma,

and RNA sequencing revealed a fusion of the ZCCHC8 and ROS1 genes resulting from the translocation of chromosomes 6 and 12. After fifteen months of treatment, the tumor continued to grow and metastases appeared. After consultation and obtaining a consent from the child's parents, treatment with the ROS1 tyrosine kinase inhibitor Entrectinib was initiated. Remarkably, within a month from starting this targeted therapy, the tumor size significantly decreased [44].

While this case represents a notable success, it remains an exception in the current landscape of targeted cancer therapy. Presently, targeted therapies are predominantly developed for diseases characterized by point mutations or gene fusions resulting in chimeric proteins. This is mostly due to the limitations of existing detection methods, which are less adept at identifying balanced chromosomal rearrangements, particularly those occurring in non-coding regions. Analysis of FFPE samples using Hi-C is capable of detecting not only chromosomal rearrangements leading to gene fusions, but also those that occur in non-coding regions and can disrupt regulatory element, which might alter oncogene expression [45]. The application of the Hi-C technique developed by us offers an extension of already existing high-throughput sequencing methods. By enabling detection of a broader range of genomic alterations, it allows researchers to uncover clinically relevant information that might otherwise remain elusive. This comprehensive genomic insight is instrumental not only in promoting our understanding of tumor biology, but also in identifying novel therapeutic targets.

Supplementary information. The online version contains supplementary material available at https://doi.org/10.1134/S0006297924040047.

Acknowledgments. We express our gratitude to the Ministry of Science and Higher Education of the Russian Federation (state project FWNR-2022-0019) for providing access to computing power. Access to the public resources and datasets was provided by Novosibirsk State University with the support of the Minis Ministry of Science and Higher Education of the Russian Federation (grant no. 2019-0546; FSUS-2024-0018).

Contributions. M.M.G. and V.S.F. developed the concept and managed the study; M.M.G., Ya.K.S., M.A.N., T.A.L., N.Yu.T., A.A.S., A.I.R., N.V.V., S.V.V., T.S.G., E.V.D., and M.A.T. conducted experiments; M.M.G., V.S.F., E.V.D., and M.A.K. discussed the results; M.M.G. and Ya.K.S. wrote the manuscript; V.S.F. edited the text of the article.

Funding. The research was supported by the Russian Science Foundation (project no. 22-24-00190).

Ethics declarations. This study was performed in line with the principles of the Declaration of Helsinki. Approval was granted by the Research Ethics Committee of the Research Institute of Medical Genetics, Tomsk National Research Medical Center (27.07.2017/no. 106). All study participants provided informed consent. The authors of this work declare that they have no conflicts of interest.

REFERENCES

1. Schmitz, R., Ceribelli, M., Pittaluga, S., Wright, G., and Staudt, L. M. (2014) Oncogenic mechanisms in Burkitt lymphoma, *Cold Spring Harb. Perspect. Med.*, **4**, a014282, doi: 10.1101/cshperspect.a014282.
2. Kumar-Sinha, C., Tomlins, S. A., and Chinnaiyan, A. M. (2008) Recurrent gene fusions in prostate cancer, *Nat. Rev. Cancer*, **8**, 497-511, doi: 10.1038/nrc2402.
3. Pflueger, D., Rickman, D. S., Sboner, A., Perner, S., LaFargue, C. J., Svensson, M. A., Moss, B. J., Kitabayashi, N., Pan, Y., de la Taille, A., Kuefer, R., Tewari, A. K., Demichelis, F., Chee, M. S., Gerstein, M. B., and Rubin, M. A. (2009) N-Myc downstream regulated gene 1 (NDRG1) is fused to ERG in prostate cancer, *Neoplasia*, **11**, 804-811, doi: 10.1593/neo.09572.
4. Sorensen, P. H., Lessnick, S. L., Lopez-Terrada, D., Liu, X. F., Triche, T. J., and Denny, C. T. (1994) A second Ewing's sarcoma translocation, t(21,22), fuses the EWS gene to another ETS-family transcription factor, ERG, *Nat. Genet.*, **6**, 146-151, doi: 10.1038/ng0294-146.
5. Sotoca, A. M., Prange, K. H. M., Reijnders, B., Mandoli, A., Nguyen, L. N., Stunnenberg, H. G., and Martens, J. H. A. (2016) The oncofusion protein FUS-ERG targets key hematopoietic regulators and modulates the all-trans retinoic acid signaling pathway in t(16,21) acute myeloid leukemia, *Oncogene*, **35**, 1965-1976, doi: 10.1038/onc.2015.261.
6. Persson, M., Andrén, Y., Mark, J., Horlings, H. M., Persson, F., and Stenman, G. (2009) Recurrent fusion of MYB and NFIB transcription factor genes in carcinomas of the breast and head and neck, *Proc. Natl. Acad. Sci. USA*, **106**, 18740-18744, doi: 10.1073/pnas.0909114106.
7. Humtsoe, J. O., Kim, H.-S., Jones, L., Cevallos, J., Boileau, P., Kuo, F., Morris, L. G. T., and Ha, P. (2022) Development and characterization of MYB-NFIB fusion expression in adenoid cystic carcinoma, *Cancers*, **14**, 2263, doi: 10.3390/cancers14092263.
8. Turner, N., and Grose, R. (2010) Fibroblast growth factor signalling: from development to cancer, *Nat. Rev. Cancer*, **10**, 116-129, doi: 10.1038/nrc2780.
9. Nakanishi, Y., Akiyama, N., Tsukaguchi, T., Fujii, T., Satoh, Y., Ishii, N., and Aoki, M. (2015) Mechanism of oncogenic signal activation by the novel fusion kinase FGFR3-BAIAP2L1, *Mol. Cancer Ther.*, **14**, 704-712, doi: 10.1158/1535-7163.MCT-14-0927-T.
10. Guo, Q., Lakatos, E., Bakir, I. A., Curtius, K., Graham, T. A., and Mustonen, V. (2022) The mutational signa-

tures of formalin fixation on the human genome, *Nat. Commun.*, **13**, 4487, doi: 10.1038/s41467-022-32041-5.

11. Scolnick, J. A., Dimon, M., Wang, I.-C., Huelga, S. C., and Amorese, D. A. (2015) An efficient method for identifying gene fusions by targeted RNA sequencing from fresh frozen and FFPE samples, *PLoS One*, **10**, e0128916, doi: 10.1371/journal.pone.0128916.
12. Mardis, E. R., and Wilson, R. K. (2009) Cancer genome sequencing: a review, *Hum. Mol. Genet.*, **18**, 163-168, doi: 10.1093/hmg/ddp396.
13. Maher, C. A., Kumar-Sinha, C., Cao, X., Kalyana-Sundaram, S., Han, B., Jing, X., Sam, L., Barrette, T., Palanisamy, N., and Chinnaiyan, A. M. (2009) Transcriptome sequencing to detect gene fusions in cancer, *Nature*, **458**, 97-101, doi: 10.1038/nature07638.
14. Peng, H., Huang, R., Wang, K., Wang, C., Li, B., Guo, Y., Li, M., Zhang, D., Dong, H., Chen, H., Chen, C., Xu, Q., Li, F., Tian, L., and Wu, J. (2021) Development and validation of an RNA sequencing assay for gene fusion detection in formalin-fixed, paraffin-embedded tumors, *J. Mol. Diagn.*, **23**, 223-233, doi: 10.1016/j.jmoldx.2020.11.005.
15. Ahlfen, S. vo., Missel, A., Bendrat, K., and Schlumpberger, M. (2007) Determinants of RNA quality from FFPE samples, *PLoS One*, **2**, e1261, doi: 10.1371/journal.pone.0001261.
16. Groelz, D., Sobin, L., Branton, P., Compton, C., Wyrich, R., and Rainen, L. (2013) Non-formalin fixative versus formalin-fixed tissue: a comparison of histology and RNA quality, *Exp. Mol. Pathol.*, **94**, 188-194, doi: 10.1016/j.yexmp.2012.07.002.
17. Wang, X., Xu, J., Zhang, B., Hou, Y., Song, F., Lyu, H., and Yue, F. (2021) Genome-wide detection of enhancer-hijacking events from chromatin interaction data in re-arranged genomes, *Nat. Methods*, **18**, 661-668, doi: 10.1038/s41592-021-01164-w.
18. Engreitz, J. M., Agarwala, V., and Mirny, L. A. (2012) Three-dimensional genome architecture influences partner selection for chromosomal translocations in human disease, *PLoS One*, **7**, e44196, doi: 10.1371/journal.pone.0044196.
19. Harewood, L., Kishore, K., Eldridge, M. D., Wingett, S., Pearson, D., Schoenfelder, S., Collins, V. P., and Fraser, P. (2017) Hi-C as a tool for precise detection and characterisation of chromosomal rearrangements and copy number variation in human tumours, *Genome Biol.*, **18**, 125, doi: 10.1186/s13059-017-1253-8.
20. Chakraborty, A., and Ay, F. (2017) Identification of copy number variations and translocations in cancer cells from Hi-C data, *Bioinformatics*, **34**, 338-345, doi: 10.1093/bioinformatics/btx664.
21. Dixon, J. R., Xu, J., Dileep, V., Zhan, Y., Song, F., Le, V. T., Yardımcı, G. G., Chakraborty, A., Bann, D. V., Wang, Y., Clark, R., Zhang, L., Yang, H., Liu, T., Iyyanki, S., An, L., Pool, C., Sasaki, T., Rivera-Mulia, J. C., Ozadam, H., Lajoie, B. R., Kaul, R., Buckley, M., Lee, K., Diegel, M., Pezic, D., Ernst, C., Hadjur, S., Odom, D. T., Stamatoyannopoulos, J. A., Broach, J. R., Hardison, R. C., Ay, F., Noble, W. S., Dekker, J., Gilbert, D. M., and Yue, F. (2018) Integrative detection and analysis of structural variation in cancer genomes, *Nat. Genet.*, **50**, 1388-1398, doi: 10.1038/s41588-018-0195-8.
22. Melo, U. S., Schöpflin, R., Acuna-Hidalgo, R., Mensah, M. A., Fischer-Zirnsak, B., Holtgrewe, M., Klever, M.-K., Türkmen, S., Heinrich, V., Pluym, I. D., Matoso, E., Bernardo de Sousa, S., Louro, P., Hülsemann, W., Cohen, M., Dufke, A., Latos-Bieleńska, A., Vingron, M., Kalscheuer, V., Quintero-Rivera, F., Spielmann, M., and Mundlos, S. (2020) Hi-C identifies complex genomic rearrangements and TAD-shuffling in developmental diseases, *Am. J. Hum. Genet.*, **106**, 872-884, doi: 10.1016/j.ajhg.2020.04.016.
23. Adeel, M. M., Rehman, K., Zhang, Y., Arega, Y., and Li, G. (2022) Chromosomal translocations detection in cancer cells using chromosomal conformation capture data, *Genes*, **13**, 1170, doi: 10.3390/genes13071170.
24. Du, Y., Gu, Z., Li, Z., Yuan, Z., Zhao, Y., Zheng, X., Bo, X., Chen, H., and Wang, C. (2022) Dynamic interplay between structural variations and 3D genome organization in pancreatic cancer, *Adv. Sci.*, **9**, 2200818, doi: 10.1002/advs.202200818.
25. Kim, K., Kim, M., Kim, Y., Lee, D., and Jung, I. (2022) Hi-C as a molecular rangefinder to examine genomic rearrangements, *Semin. Cell Dev. Biol.*, **121**, 161-170, doi: 10.1016/j.semcdb.2021.04.024.
26. Song, F., Xu, J., Dixon, J., and Yue, F. (2022) Analysis of Hi-C data for discovery of structural variations in cancer, *Methods Mol. Biol.*, **2301**, 143-161, doi: 10.1007/978-1-0716-1390-0_7.
27. Sidiropoulos, N., Mardin, B. R., Rodríguez-González, F. G., Bochkov, I. D., Garg, S., Stütz, A. M., Korbel, J. O., Aiden, E. L., and Weischenfeldt, J. (2022) Somatic structural variant formation is guided by and influences genome architecture, *Genome Res.*, **32**, 643-655, doi: 10.1101/gr.275790.121.
28. Troll, C. J., Putnam, N. H., Hartley, P. D., Rice, B., Blanchette, M., Siddiqui, S., Ganbat, J.-O., Powers, M. P., Ramakrishnan, R., Kunder, C. A., Bustamante, C. D., Zehnder, J. L., Green, R. E., and Costa, H. A. (2019) Structural variation detection by proximity ligation from formalin-fixed, paraffin-embedded tumor tissue, *J. Mol. Diagn.*, **21**, 375-383, doi: 10.1016/j.jmoldx.2018.11.003.
29. Allahyar, A., Pieterse, M., Swennenhuis, J., Los-de Vries, G. T., Yilmaz, M., Leguit, R., Meijers, R. W. J., van der Geize, R., Vermaat, J., Cleven, A., van Wezel, T., Diepstra, A., van Kempen, L. C., Hijmering, N. J., Stathi, P., Sharma, M., Melquiond, A. S. J., de Vree, P. J. P., Verstegen, M. J. A. M., Krijger, P. H. L., Hajo, K., Simonis, M., Rakszewska, A., van Min, M., de Jong, D., Ylstra, B., Feitsma, H., Splinter, E., and de Laat, W. (2021) Robust detection of translocations in lymphoma FFPE

samples using targeted locus capture-based sequencing, *Nat. Commun.*, **12**, 3361, doi: 10.1038/s41467-021-23695-8.
30. Gridina, M., Popov, A., Shadskiy, A., Torgunakov, N., Kechin, A., Khrapov, E., Ryzhkova, O., Filipenko, M., and Fishman, V. (2023) Expanding the list of sequence-agnostic enzymes for chromatin conformation capture assays with S1 nuclease, *bioRxiv*, doi: 10.1101/2023.06.15.545138.
31. Gridina, M., Mozheiko, E., Valeev, E., Nazarenko, L. P., Lopatkina, M. E., Markova, Z. G., Yablonskaya, M. I., Voinova, V. Y., Shilova, N. V., Lebedev, I. N., and Fishman, V. (2021) A cookbook for DNase Hi-C, *Epigenet. Chromatin*, **14**, 15, doi: 10.1186/s13072-021-00389-5.
32. Rao, S. S. P., Huntley, M. H., Durand, N. C., Stamenova, E. K., Bochkov, I. D., Robinson, J. T., Sanborn, A. L., Machol, I., Omer, A. D., Lander, E. S., and Aiden, E. L. (2014) A 3D map of the human genome at kilobase resolution reveals principles of chromatin looping, *Cell*, **159**, 1665-1680, doi: 10.1016/j.cell.2014.11.021.
33. Belaghzal, H., Dekker, J., and Gibcus, J. H. (2017) Hi-C 2.0: An optimized Hi-C procedure for high-resolution genome-wide mapping of chromosome conformation, *Methods*, **123**, 56-65, doi: 10.1016/j.ymeth.2017.04.004.
34. Zheng, W., Yang, Z., Ge, X., Feng, Y., Wang, Y., Liu, C., Luan, Y., Cai, K., Vakal, S., You, F., Guo, W., Wang, W., Feng, Z., and Li, F. (2021) Freeze substitution Hi-C, a convenient and cost-effective method for capturing the natural 3D chromatin conformation from frozen samples, *J. Genet. Genomics*, **48**, 237-247, doi: 10.1016/j.jgg.2020.11.002.
35. Golloshi, R., Sanders, J. T., and McCord, R. P. (2018) Iteratively improving Hi-C experiments one step at a time, *Methods*, **142**, 47-58, doi: 10.1016/j.ymeth.2018.04.033.
36. Lafontaine, D. L., Yang, L., Dekker, J., and Gibcus, J. H. (2021) Hi-C 3.0: improved protocol for genome-wide chromosome conformation capture, *Curr. Protoc.*, **1**, e198, doi: 10.1002/cpz1.198.
37. Akgol Oksuz, B., Yang, L., Abraham, S., Venev, S. V., Krietenstein, N., Parsi, K. M., Ozadam, H., Oomen, M. E., Nand, A., Mao, H., Genga, R. M. J., Maehr, R., Rando, O. J., Mirny, L. A., Gibcus, J. H., and Dekker, J. (2021) Systematic evaluation of chromosome conformation capture assays, *Nat. Methods*, **18**, 1046-1055, doi: 10.1038/s41592-021-01248-7.
38. Kennedy-Darling, J., and Smith, L. M. (2014) Measuring the formaldehyde protein-DNA cross-link reversal rate, *Anal. Chem.*, **86**, 5678-5681, doi: 10.1021/ac501354y.
39. Einaga, N., Yoshida, A., Noda, H., Suemitsu, M., Nakayama, Y., Sakurada, A., Kawaji, Y., Yamaguchi, H., Sasaki, Y., Tokino, T., and Esumi, M. (2017) Assessment of the quality of DNA from various formalin-fixed paraffin-embedded (FFPE) tissues and the use of this DNA for next-generation sequencing (NGS) with no artifactual mutation, *PLoS One*, **12**, e0176280, doi: 10.1371/journal.pone.0176280.
40. Kuwata, T., Wakabayashi, M., Hatanaka, Y., Morii, E., Oda, Y., Taguchi, K., Noguchi, M., Ishikawa, Y., Nakajima, T., Sekine, S., Nomura, S., Okamoto, W., Fujii, S., and Yoshino, T. (2020) Impact of DNA integrity on the success rate of tissue-based next-generation sequencing: lessons from nationwide cancer genome screening project SCRUM-Japan GI-SCREEN, *Pathol. Int.*, **70**, 932-942, doi: 10.1111/pin.13029.
41. Ma, W., Ay, F., Lee, C., Gulsoy, G., Deng, X., Cook, S., Hesson, J., Cavanaugh, C., Ware, C. B., Krumm, A., Shendure, J., Blau, C. A., Disteche, C. M., Noble, W. S., and Duan, Z. (2018) Using DNase Hi-C techniques to map global and local three-dimensional genome architecture at high resolution, *Methods*, **142**, 59-73, doi: 10.1016/j.ymeth.2018.01.014.
42. Lomov, N., Zerkalenkova, E., Lebedeva, S., Viushkov, V., and Rubtsov, M. A. (2021) Cytogenetic and molecular genetic methods for chromosomal translocations detection with reference to the KMT2A/MLL gene, *Crit. Rev. Clin. Lab. Sci.*, **58**, 180-206, doi: 10.1080/10408363.2020.1844135.
43. Mosele, F., Remon, J., Mateo, J., Westphalen, C. B., Barlesi, F., Lolkema, M. P., Normanno, N., Scarpa, A., Robson, M., Meric-Bernstam, F., Wagle, N., Stenzinger, A., Bonastre, J., Bayle, A., Michiels, S., Bièche, I., Rouleau, E., Jezdic, S., Douillard, J.-Y., Reis-Filho, J. S., Dienstmann, R., and André, F. (2020) Recommendations for the use of next-generation sequencing (NGS) for patients with metastatic cancers: a report from the ESMO precision medicine working group, *Ann. Oncol.*, **31**, 1491-1505, doi: 10.1016/j.annonc.2020.07.014.
44. Hehir-Kwa, J. Y., Koudijs, M. J., Verwiel, E. T. P., Kester, L. A., van Tuil, M., Strengman, E., Buijs, A., Kranendonk, M. E. G., Hiemcke-Jiwa, L. S., de Haas, V., van de Geer, E., de Leng, W., van der Lugt, J., Lijnzaad, P., Holstege, F. C. P., Kemmeren, P., and Tops, B. B. J. (2022) Improved gene fusion detection in childhood cancer diagnostics using RNA sequencing, *JCO Precis. Oncol.*, **6**, e2000504, doi: 10.1200/PO.20.00504.
45. Zhang, Y., Chen, F., and Creighton, C. J. (2021) SVExpress: identifying gene features altered recurrently in expression with nearby structural variant breakpoints, *BMC Bioinformatics*, **22**, 135, doi: 10.1186/s12859-021-04072-0.